

A universal speed limit for spreading of quantum coherence

Gevorg Martirosyan,* Martin Gazo, Jiří Etrych, Simon M. Fischer,

Sebastian J. Morris, Christopher J. Ho, Christoph Eigen, and Zoran Hadzibabic

Cavendish Laboratory, University of Cambridge, J. J. Thomson Avenue, Cambridge CB3 0HE, United Kingdom

(Dated: November 1, 2024)

Discoveries of fundamental limits for the rates of physical processes, from the speed of light to the Lieb–Robinson bound for information propagation [1–4], are conceptual breakthroughs that often challenge our understanding of the underlying physics. Here we observe such a limit for a paradigmatic many-body phenomenon, the spreading of coherence during formation of a weakly interacting Bose–Einstein condensate [5–21]. We study condensate formation in an isolated homogeneous atomic gas [22, 23] that is initially far from equilibrium, in an incoherent low-energy state, and condenses as it relaxes towards equilibrium. Tuning the inter-atomic interactions that drive condensation, we show that the spreading of coherence through the system is initially slower for weaker interactions, and faster for stronger ones, but always eventually reaches the same limit, where the square of the coherence length grows at a universal rate given by the ratio of Planck’s constant and the particle mass. These observations are robust to changes in the initial state, the gas density, and the system size. Our results provide benchmarks for theories of universality far from equilibrium [24–30], are relevant for quantum technologies that rely on large-scale coherence, and invite similar measurements in other quantum systems.

Understanding the dynamics of far-from-equilibrium many-body systems, including the emergence of long-range order in such systems, is an outstanding problem in physics, relevant from subnuclear to cosmological lengthscales [24–30]. The theoretical framework of nonthermal fixed points (NTFPs) [25] generalises the concepts from the equilibrium theory of continuous phase transitions, and posits that far-from-equilibrium dynamics have similarly universal properties. At the transition to an ordered state of matter, such as a superfluid or a ferromagnet, the system is scale invariant and its salient properties do not depend on the microscopic details [31]. Analogously, in the NTFP theory, far-from-equilibrium systems, including the early universe undergoing reheating [32], quark-gluon plasma in heavy-ion collisions [33], quantum magnets [34], and ultracold atomic gases [35–40], generically display dynamic (spatiotemporal) scaling, with scaling exponents that could define far-from-equilibrium universality classes. Recently, far-from-equilibrium dynamic scaling was observed in several experiments with ultracold atoms [41–45].

Beyond the elegant scaling properties of far-from-equilibrium dynamics, a crucial question is how quickly long-range order can be established in a quantum system. Here we study this problem for the formation of a paradigmatic macroscopically coherent state, the Bose–Einstein condensate.

We study condensate formation in an isolated homogeneous three-dimensional Bose gas [22, 23] that we prepare in various far-from-equilibrium initial states. The gas is initially incoherent, but has very low energy, and condenses as it relaxes towards equilibrium under the influence of inter-atomic interactions, characterised by the s -wave scattering length a . As illustrated in Fig. 1a, in a homogeneous system the (global) condensate grows through coarsening, the local spreading of coherence. This coarsening corresponds to narrowing of the momentum distribution $n_k(k)$ (where k is the wavenumber) and is quantified by the growth of the coherence length ℓ .

Starting from a generic far-from-equilibrium state, the initial dynamics cannot be universal, but long-time coarsening

in an isolated system is predicted to feature universal self-similar dynamic scaling of the low- k momentum distribution [36, 38]:

$$n_k(k, t) = \ell_0^d \left(\frac{t}{t_0} \right)^\alpha f \left[\left(\frac{t}{t_0} \right)^\beta k \ell_0 \right] = \ell^d(t) f[k\ell(t)], \quad (1)$$

where d is the system dimensionality, f a dimensionless scaling function, and α and β the scaling exponents, with $\alpha = d\beta$; the coherence length is $\ell = (t/t_0)^\beta \ell_0$, where t_0 is an arbitrary reference time and $\ell_0 \equiv \ell(t_0)$. The condensate growth is given by $n_0(t)$, where $n_0 \equiv n_k(k=0)$, and for $d=3$, from Eq. (1), $n_0 \propto \ell^3$. In general, Eq. (1) holds only asymptotically for $t \rightarrow \infty$. However, the same scaling can be observed at finite times, with the only relic of the non-universal initial dynamics being a time shift $t \rightarrow t - t^*$, where t^* depends on the initial state [45] (see also [46]).

For $\ell \propto t^\beta$, or rather $\ell \propto (t - t^*)^\beta$, a natural way to define a time-invariant ‘speed of coarsening’ is $D \equiv d\ell^{1/\beta}/dt$, which also eliminates the non-universal t^* . The absolute value of D depends on the dimensionless factors in the definition of ℓ , which, for concreteness, we define such that for an equilibrium condensate ℓ^3 is equal to the system volume.

For a low-energy weakly interacting Bose gas, described by the Gross–Pitaevskii equation (GPE), the interaction-set units of length and time are, respectively, $\xi = 1/\sqrt{8\pi na}$ and $t_\xi \equiv m\xi^2/\hbar$, where n is the gas density, \hbar the reduced Planck’s constant, and m the atom mass; ξ is the equilibrium correlation (healing) length at zero temperature, and in this context the gas is weakly interacting for any $na^3 \ll 1$. Hence, for any β , on dimensional grounds $\ell/\xi \propto [(t - t^*)/t_\xi]^\beta$ and

$$D \propto \frac{\xi^{1/\beta}}{t_\xi} \propto \frac{\hbar}{m} (na)^{1-1/(2\beta)}. \quad (2)$$

The theory [36, 38] predicts $\beta = 1/2$, which has a counter-intuitive implication that the speed of coarsening, $D = d\ell^2/dt \sim \hbar/m$, does not depend on the strength of the interactions that drive it (see also [47]).

Here we verify the scaling-theory predictions, measure a universal $D = 3.0(2)\hbar/m$ for a range of interaction strengths,

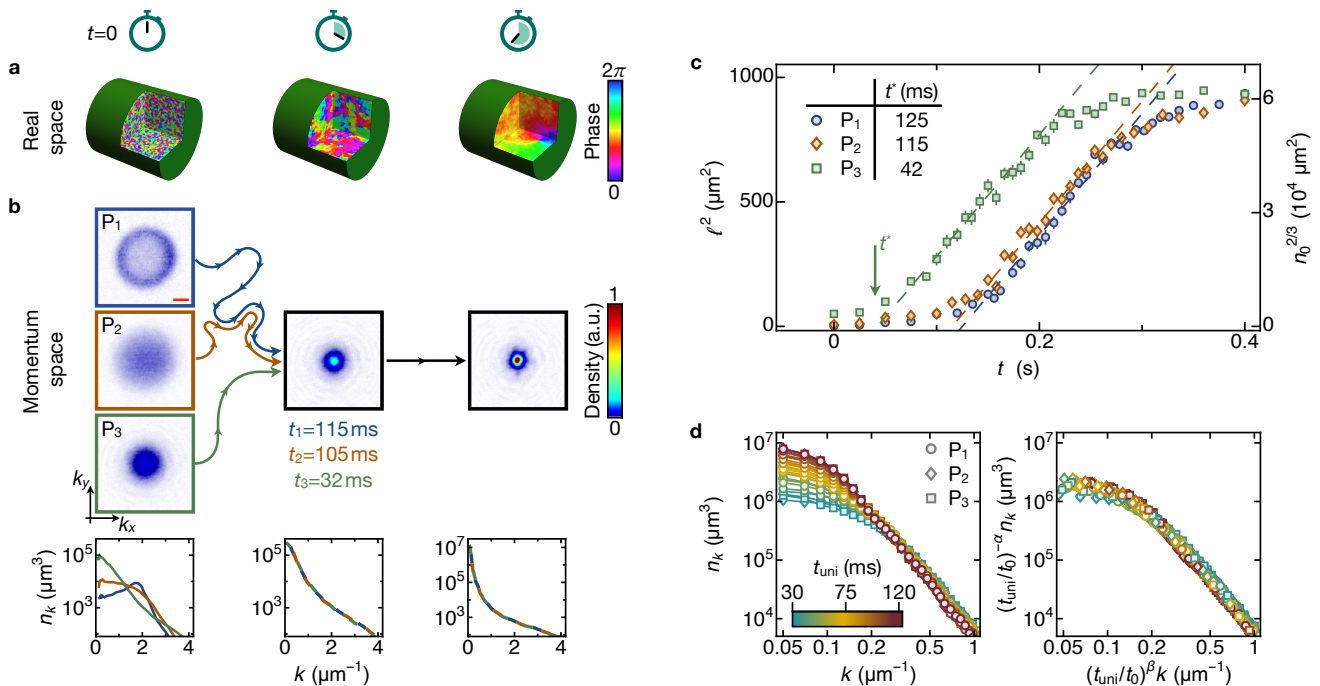


FIG. 1. **Universal coarsening of an isolated Bose gas.** **a**, Real-space cartoon of coarsening. **b**, Momentum-space relaxation for different far-from-equilibrium initial states. Our initial states $P_{1,2,3}$ (left column) have different momentum distributions n_k , but the same energy, so the gas always relaxes towards the same equilibrium state. For $P_{1,2,3}$, the system takes different times, $t_{1,2,3}$, to evolve to the same n_k shown in the middle column (the plot shows three indistinguishable curves), but from this point onwards it always evolves in the same way. All n_k distributions are averages of at least 20 experimental repetitions and the red scale bar in the top image shows $1 \mu\text{m}^{-1}$. **c**, Growth of the coherence length, $\ell \propto n_0^{1/3}$, where $n_0 \equiv n_k(k=0)$ quantifies the condensate occupation. Plotting ℓ^2 versus t reveals three stages of relaxation: (i) the non-universal initial dynamics, (ii) the scaling regime where ℓ^2 grows linearly (dashed lines), as expected for the scaling exponent $\beta = 1/2$, and (iii) the breakdown of scaling at long times due to finite-size effects. The curves for $P_{1,2,3}$ are parallel, with the initial-state effects captured by the different time offsets t^* (intercepts of the dashed lines). The slopes of the dashed lines are $D = d\ell^2/dt \approx 3\hbar/m$. **d**, Dynamic scaling. In the regime where ℓ shows the expected scaling, the full low- k distributions for all three initial states (left panel) can be dynamically scaled onto the same universal curve (right panel) according to Eq. (1) with $t \rightarrow t_{\text{uni}} \equiv t - t^*$ and the predicted $\alpha = 3\beta = 3/2$; $t_0 = 50$ ms is an arbitrary reference time. All error bars show standard errors of the measurements.

and establish the conditions for observing this long-time ‘speed limit’ for the spreading of coherence.

Our experiments are performed with ^{39}K atoms in a cylindrical optical box trap, such as sketched in Fig. 1a [22, 48] (Methods). Our box volume is $V = 61 \times 10^3 \mu\text{m}^3$, our $n = 4.9 \mu\text{m}^{-3}$ corresponds to the critical temperature for condensation $T_c = 120$ nK, and we tune a using a Feshbach resonance. To test the robustness of our observations, we engineer three different far-from-equilibrium initial states (see Fig. 1b), by starting with a quasi-pure condensate and using a time-varying force to perturb the cloud (see Extended Data Fig. 1 and Methods). These initial states have no condensed component (no global coherence), and have different n_k distributions, but the same low energy per particle, $\varepsilon = k_B \times 20$ nK $\ll k_B T_c$, where k_B is the Boltzmann constant. Hence, the system always relaxes towards the same equilibrium state that has a large condensed fraction (about 60%).

At $t = 0$ the gas is non-interacting, and we initiate relaxation by turning on the interactions, with a in the range (50 – 600) a_0 , where a_0 is the Bohr radius. For our n and range of a , corresponding to $na^3 < 2 \times 10^{-4}$, the particle loss due to three-body recombination is much slower than the spreading of coherence (see Methods), so coarsening oc-

curs in an essentially isolated system.

We measure $n_k(k, t)$ by absorption imaging after time-of-flight expansion, performing the inverse-Abel transform on the line-of-sight integrated distributions and averaging over at least 20 experimental repetitions; note that just for the images shown in Figs. 1b and 2a we instead image only slices of the cloud [49] corresponding to $k_z \approx 0$.

We normalise n_k such that $\int n_k 4\pi k^2 dk = N$, where N is the total atom number. The condensate occupation is then $N_0 = (2\pi)^3 n_0/V$. Since $\ell \propto n_0^{1/3}$ [see Eq. (1)], we define $\ell \equiv (Vn_0/n_0^{\text{eq}})^{1/3}$, where n_0^{eq} is the equilibrium value of n_0 , so $\ell^3 = V$ for $n_0 = n_0^{\text{eq}}$. For $n_k = \ell^3 f[k\ell]$, the value of ℓ fully specifies the (low- k) momentum distribution; outside the scaling regime, n_k does not have the same shape, but the growth of ℓ still heuristically captures the spreading of coherence.

In Figs. 1b - 1d, we show for fixed $a = 100 a_0$ that our gas exhibits universal coarsening dynamics with the analytically predicted exponents $\alpha = 3\beta = 3/2$.

We first show, in Fig. 1b, that for our initial states $P_{1,2,3}$, shown in the left column, the long-time evolution differs only in some time offsets. Starting from an initial state, $n_k(k)$ follows some trajectory in the space of functions with the same N and ε , represented by the wiggly coloured lines.

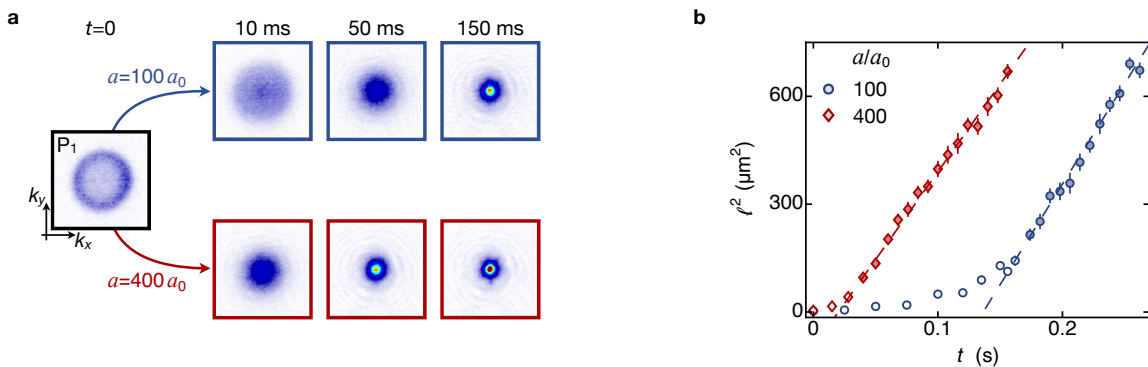


FIG. 2. **Spreading of coherence for different interaction strengths.** **a**, Gas evolution for two different interaction strengths a , starting in the same initial state P_1 . For stronger interactions, the condensate (the peak at $k = 0$) emerges sooner. **b**, However, plotting $\ell^2(t)$ shows that the interaction strength affects only the non-universal initial dynamics (open symbols), while the linear growth of ℓ^2 in the universal coarsening regime (solid symbols) is a -independent. The dashed lines show linear fits to the scaling-regime data, which both give $D \approx 3\hbar/m$ (see Fig. 3).

The middle column shows that, still far from equilibrium, these trajectories converge to the same n_k . The time that the gas takes to evolve to this n_k depends on the initial state ($t_{i=1,2,3}$ for $P_{i=1,2,3}$), but further evolution from this n_k is necessarily the same for all initial states. Note that the state trajectories for P_1 and P_2 merge before merging with the P_3 one, but we just show an n_k where all three have converged.

In Fig. 1c we plot $\ell^2(t) \propto n_0^{2/3}(t)$, which reveals the scaling regime and the time offsets t^* for $P_{1,2,3}$; for $\beta = 1/2$, in the scaling regime $\ell^2 \propto t - t^*$ (see also Extended Data Fig. 2 in Methods). This regime is highlighted by the parallel dashed lines, with slopes $D = d\ell^2/dt \approx 3\hbar/m$ that do not depend on the initial state, and intercepts that give the three t^* values. At long times, as the system approaches equilibrium ($\ell^3 \gtrsim V/3$), this scaling breaks down due to finite-size effects.

In Fig. 1d, using the t^* values from Fig. 1c, we show that in the scaling regime the low- k distributions for all three initial states can be collapsed onto the same universal curve according to Eq. (1), with $\alpha = 3\beta = 3/2$ and $t \rightarrow t - t^*$.

We now turn to varying the strength of the interactions that drive the coarsening. In Fig. 2 we show, for the same initial state, measurements for $a = 100 a_0$ and $400 a_0$. The $100 a_0$ data here is the same as in Fig. 1, and we focus on the regime $\ell^2 < 700 \mu\text{m}^2$, before the finite-size saturation of ℓ occurs.

The images in Fig. 2a show what one intuitively expects – for larger a the condensate emerges sooner. However, in Fig. 2b, plotting $\ell^2(t)$ reveals that the effects of the interaction strength are, just like the initial-state effects, confined to the difference in the non-universal t^* , and in the scaling regime the slopes $D \approx 3\hbar/m$ are essentially the same; here the dashed lines show independent fits to the scaling-regime data indicated by the solid symbols.

We performed such measurements for various interaction strengths, and also varied the gas density and system size. As we show in Fig. 3, we observe no systematic variation of D and get a combined estimate $D = 3.0(2)\hbar/m$.

Finally, in Fig. 4 we study how the system approaches the long-time coarsening speed D , which also reconciles our ob-

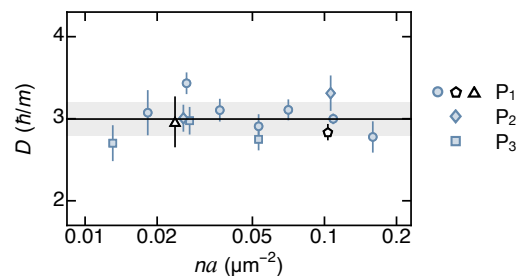


FIG. 3. **Universality of the coarsening speed D .** Our measurements for various interaction strengths show no systematic variation of D , and give a combined estimate $D = 3.0(2)\hbar/m$ (solid line and shading). The open pentagon indicates a measurement where we also varied the system volume V , reducing it by a factor of 4, while keeping the gas density, and hence T_c and the equilibrium condensed fraction, the same; in this case ℓ^2 saturates at a correspondingly lower value ($\propto V^{2/3}$), but D is not affected. The open triangle indicates a measurement where we instead reduced the gas density by a factor of 4; this reduces $T_c \propto n^{2/3}$ and the equilibrium condensed fraction (from about 60% to about 30%), but again D is not affected (see also Extended Data Fig. 3 in Methods).

servations with the finite-system intuition (and experience) that for stronger interactions condensates form faster, and for $a \rightarrow 0$ they do not form at all.

As we illustrate in Fig. 4a for fixed n , the same initial state (P_1), and three values of a , for weaker interactions the gas takes longer to join the universal scaling trajectory, and joins it at a larger value of ℓ . Here all curves start at $t = 0$ and plotting versus $t - t^*$ collapses them in the scaling regime; the dashed line shows $\ell^2 = 3\hbar(t - t^*)/m$.

In Fig. 4b we show that the timescale for the approach to the scaling regime is set by $t_\xi \propto 1/(na)$. Here, expressing all our P_1 data for different a , n , and V (see Fig. 3) in terms of ξ and t_ξ collapses them onto a single curve, and the inset shows that the approach to the scaling regime is captured well by an exponential with a time constant $\tau \approx 50 t_\xi$ (see also Extended Data Fig. 4 in Methods). Numerically differentiating these data, and thus eliminating the non-universal t^* , in Fig. 4c we show how $d\ell^2/dt$ approaches the univer-

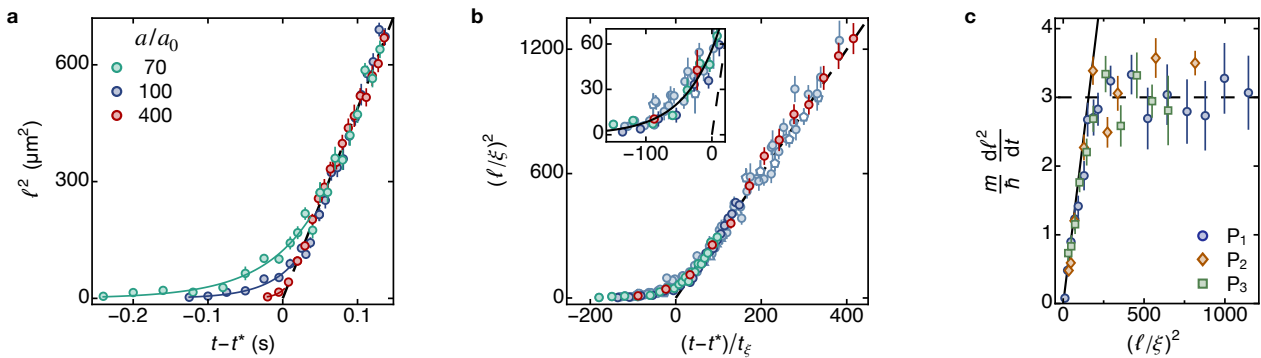


FIG. 4. **Reaching the coarsening speed limit.** **a**, The growth of ℓ^2 for the same initial state (P_1) and gas density n , but different interaction strengths. All curves start at $t = 0$ and plotting them versus $t - t^*$ (with a -dependent t^*) collapses them in the universal scaling regime. The dashed line shows $\ell^2 = 3\hbar(t - t^*)/m$. For weaker interactions the system approaches this speed limit slower, and reaches it at a larger ℓ ; the solid lines show exponential fits to the early-time data. **b**, When expressed in the interactions-set units of length, $\xi = 1/\sqrt{8\pi na}$, and time, $t_\xi \equiv m\xi^2/\hbar$, the data from **a**, and all our other P_1 data (light blue symbols) for different a , n , and V (see Fig. 3), collapse onto a single curve. The inset shows that the approach to the scaling regime is captured well by an exponential with a time constant $\tau \approx 50 t_\xi$ (solid line). **c**, Numerically differentiating the data in **b**, and similar curves for the initial states P_2 and P_3 , we eliminate the non-universal t^* values and show as a function of $(\ell/\xi)^2$ how $d\ell^2/dt$ approaches the universal $D = 3\hbar/m$ and then stops growing. This speed limit is always reached at the same ℓ/ξ , but for weaker interactions (larger ξ), observing this requires a larger physical system. The solid and dashed line, respectively, correspond to the solid and dashed line in **b**.

sal $D = 3\hbar/m$ as a function of $(\ell/\xi)^2$; here we also add the corresponding data for the initial states P_2 and P_3 .

The dimensionless results in Figs. 4**b** and 4**c** imply that for any interaction strength the system would eventually reach the same coarsening speed D . However, consistently with the NTFP theory [38], this speed limit is reached for $\ell \gg \xi$. Hence, the system size required to observe this is larger for larger ξ (smaller na), and diverges for $na \rightarrow 0$. As we discuss in Methods and Extended Data Fig. 5, previous experiments on the emergence of extended coherence during far-from-equilibrium condensation, in both harmonic [16] and box [43] traps, were not in the universal-speed regime; consequently, for tunable interactions in Ref. [43], the observed relaxation time was $\propto 1/a$.

The speed limit $D = 3\hbar/m$ has curious implications for the emergence of coherence on truly macroscopic length-scales. For ^{39}K , for coherence to spread via coarsening over 1 cm would require hours, and for it spread through a pool-sized cloud would take centuries. Even reducing the particle mass to that of a nucleon, it would take longer than the age of the universe for coherence to spread from London to New York.

Our results should also be relevant for benchmarking the theories of ultrarelativistic systems, for which coarsening with $\beta = 1/2$ is also predicted [36]. In that case the effective particle mass, $m_{\text{eff}} \sim \hbar/(\xi c)$, where c is the speed of light, is set by an emergent low- k energy gap in the spectrum. Note that this gap is larger for stronger interactions, making $D \sim \hbar/m_{\text{eff}} \sim \xi c$ smaller.

In the future it would be interesting to perform similar measurements for fermionic superfluids and gases with long-range interactions. With fermions one could also, without the hindrance of three-body losses, explore the regime of very strong interactions, $na^3 \gtrsim 1$.

We thank Andrey Karailiev, Maciej Gałka, Timon Hilker, Robert Smith, and Tobias Donner for useful discussions and

comments on the manuscript. This work was supported by EPSRC [Grant No. EP/P009565/1], ERC (UniFlat), and STFC [Grant No. ST/T006056/1]. C. E. acknowledges support from Jesus College (Cambridge). Z. H. acknowledges support from the Royal Society Wolfson Fellowship.

* gm572@cam.ac.uk

- [1] E. H. Lieb and D. W. Robinson, The finite group velocity of quantum spin systems, *Commun. Math. Phys.* **28**, 251 (1972).
- [2] B. Nachtergaele and R. Sims, Lieb-Robinson bounds and the exponential clustering theorem, *Commun. Math. Phys.* **265**, 119 (2006).
- [3] M. B. Hastings and T. Koma, Spectral gap and exponential decay of correlations, *Commun. Math. Phys.* **265**, 781 (2006).
- [4] S. Bravyi, M. B. Hastings, and F. Verstraete, Lieb-Robinson Bounds and the Generation of Correlations and Topological Quantum Order, *Phys. Rev. Lett.* **97**, 050401 (2006).
- [5] D. W. Snoke and J. P. Wolfe, Population dynamics of a Bose gas near saturation, *Phys. Rev. B* **39**, 4030 (1989).
- [6] H. T. C. Stoof, Formation of the condensate in a dilute Bose gas, *Phys. Rev. Lett.* **66**, 3148 (1991).
- [7] B. V. Svistunov, Highly nonequilibrium Bose condensation in a weakly interacting gas, *J. Moscow Phys. Soc.* **1**, 373 (1991).
- [8] Y. Kagan, B. V. Svistunov, and G. V. Shlyapnikov, Kinetics of Bose condensation in an interacting Bose gas, *Sov. Phys. JETP* **75**, 387 (1992).
- [9] D. V. Semikoz and I. I. Tkachev, Kinetics of Bose Condensation, *Phys. Rev. Lett.* **74**, 3093 (1995).
- [10] Y. Kagan, Kinetics of Bose-Einstein Condensate Formation in an Interacting Bose Gas, in *Bose-Einstein Condensation*, edited by A. Griffin, D. W. Snoke, and S. Stringari (Cambridge University Press, 1995).
- [11] K. Damle, S. N. Majumdar, and S. Sachdev, Phase ordering kinetics of the Bose gas, *Phys. Rev. A* **54**, 5037 (1996).
- [12] C. W. Gardiner, P. Zoller, R. J. Ballagh, and M. J. Davis, Kinetics of Bose-Einstein Condensation in a Trap, *Phys. Rev. Lett.* **79**, 1793 (1997).

- [13] H.-J. Miesner, D. M. Stamper-Kurn, M. R. Andrews, D. S. Durfee, S. Inouye, and W. Ketterle, Bosonic Stimulation in the Formation of a Bose-Einstein Condensate, *Science* **279**, 1005 (1998).
- [14] N. G. Berloff and B. V. Svistunov, Scenario of strongly nonequilibrated Bose-Einstein condensation, *Phys. Rev. A* **66**, 013603 (2002).
- [15] M. Köhl, M. J. Davis, C. W. Gardiner, T. W. Hänsch, and T. Esslinger, Growth of Bose-Einstein condensates from thermal vapor, *Phys. Rev. Lett.* **88**, 080402 (2002).
- [16] S. Ritter, A. Öttl, T. Donner, T. Bourdel, M. Köhl, and T. Esslinger, Observing the formation of long-range order during Bose-Einstein condensation, *Phys. Rev. Lett.* **98**, 090402 (2007).
- [17] M. Hugbart, J. A. Retter, A. F. Varón, P. Bouyer, A. Aspect, and M. J. Davis, Population and phase coherence during the growth of an elongated Bose-Einstein condensate, *Phys. Rev. A* **75**, 011602 (2007).
- [18] R. P. Smith, S. Beattie, S. Moulder, R. L. Campbell, and Z. Hadzibabic, Condensation dynamics in a quantum-quenched Bose gas, *Phys. Rev. Lett.* **109**, 105301 (2012).
- [19] N. Navon, A. L. Gaunt, R. P. Smith, and Z. Hadzibabic, Critical dynamics of spontaneous symmetry breaking in a homogeneous Bose gas, *Science* **347**, 167 (2015).
- [20] N. Proukakis, D. Snoke, and P. Littlewood, eds., *Universal Themes of Bose-Einstein Condensation* (Cambridge University Press, Cambridge, 2017).
- [21] N. P. Proukakis, Universality of Bose-Einstein condensation and quenched formation dynamics, in *Encyclopedia of Condensed Matter Physics (2nd Ed.)*, edited by T. Chakraborty (Academic Press, Oxford, 2024) pp. 84–123.
- [22] A. L. Gaunt, T. F. Schmidutz, I. Gotlibovych, R. P. Smith, and Z. Hadzibabic, Bose-Einstein Condensation of Atoms in a Uniform Potential, *Phys. Rev. Lett.* **110**, 200406 (2013).
- [23] N. Navon, R. P. Smith, and Z. Hadzibabic, Quantum gases in optical boxes, *Nat. Phys.* **17**, 1334 (2021).
- [24] A. J. Bray, Theory of phase-ordering kinetics, *Adv. Phys.* **51**, 481 (2002).
- [25] J. Berges, A. Rothkopf, and J. Schmidt, Nonthermal Fixed Points: Effective Weak Coupling for Strongly Correlated Systems Far from Equilibrium, *Phys. Rev. Lett.* **101**, 041603 (2008).
- [26] S. Nazarenko, *Wave turbulence* (Springer, 2011).
- [27] A. Polkovnikov, K. Sengupta, A. Silva, and M. Vengalattore, *Colloquium: Nonequilibrium dynamics of closed interacting quantum systems*, *Rev. Mod. Phys.* **83**, 863 (2011).
- [28] J. Eisert, M. Friesdorf, and C. Gogolin, Quantum many-body systems out of equilibrium, *Nat. Phys.* **11**, 124 (2015).
- [29] M. Ueda, Quantum equilibration, thermalization and prethermalization in ultracold atoms, *Nat. Rev. Phys.* **2**, 669 (2020).
- [30] J. Berges, M. P. Heller, A. Mazeliauskas, and R. Venugopalan, QCD thermalization: Ab initio approaches and interdisciplinary connections, *Rev. Mod. Phys.* **93**, 035003 (2021).
- [31] P. M. Chaikin and T. C. Lubensky, *Principles of Condensed Matter Physics* (Cambridge University Press, 1995).
- [32] R. Micha and I. I. Tkachev, Turbulent thermalization, *Phys. Rev. D* **70**, 043538 (2004).
- [33] J. Berges, K. Boguslavski, S. Schlichting, and R. Venugopalan, Turbulent thermalization process in heavy-ion collisions at ultrarelativistic energies, *Phys. Rev. D* **89**, 074011 (2014).
- [34] S. Bhattacharyya, J. F. Rodriguez-Nieva, and E. Demler, Universal Prethermal Dynamics in Heisenberg Ferromagnets, *Phys. Rev. Lett.* **125**, 230601 (2020).
- [35] B. Nowak, J. Schole, D. Sexty, and T. Gasenzer, Nonthermal fixed points, vortex statistics, and superfluid turbulence in an ultracold Bose gas, *Phys. Rev. A* **85**, 043627 (2012).
- [36] A. Piñeiro Orioli, K. Boguslavski, and J. Berges, Universal self-similar dynamics of relativistic and nonrelativistic field theories near nonthermal fixed points, *Phys. Rev. D* **92**, 025041 (2015).
- [37] J. Berges, K. Boguslavski, S. Schlichting, and R. Venugopalan, Universality Far from Equilibrium: From Superfluid Bose Gases to Heavy-Ion Collisions, *Phys. Rev. Lett.* **114**, 061601 (2015).
- [38] I. Chantesana, A. Piñeiro Orioli, and T. Gasenzer, Kinetic theory of nonthermal fixed points in a Bose gas, *Phys. Rev. A* **99**, 043620 (2019).
- [39] A. J. Groszek, P. Comaron, N. P. Proukakis, and T. P. Billam, Crossover in the dynamical critical exponent of a quenched two-dimensional Bose gas, *Phys. Rev. Res.* **3**, 013212 (2021).
- [40] A. Chatrchyan, K. T. Geier, M. K. Oberthaler, J. Berges, and P. Hauke, Analog cosmological reheating in an ultracold Bose gas, *Phys. Rev. A* **104**, 023302 (2021).
- [41] M. Prüfer, P. Kunkel, H. Strobel, S. Lannig, D. Linnemann, C.-M. Schmied, J. Berges, T. Gasenzer, and M. K. Oberthaler, Observation of universal dynamics in a spinor Bose gas far from equilibrium, *Nature* **563**, 217 (2018).
- [42] S. Erne, R. Bücker, T. Gasenzer, J. Berges, and J. Schmiedmayer, Universal dynamics in an isolated one-dimensional Bose gas far from equilibrium, *Nature* **563**, 225 (2018).
- [43] J. A. P. Glidden, C. Eigen, L. H. Dogra, T. A. Hilker, R. P. Smith, and Z. Hadzibabic, Bidirectional dynamic scaling in an isolated Bose gas far from equilibrium, *Nat. Phys.* **17**, 457 (2021).
- [44] S. Huh, K. Mukherjee, K. Kwon, J. Seo, J. Hur, S. I. Mistakidis, H. R. Sadeghpour, and J.-Y. Choi, Universality class of a spinor Bose-Einstein condensate far from equilibrium, *Nat. Phys.* **20**, 402 (2024).
- [45] M. Gazo, A. Karailiev, T. Sator, C. Eigen, M. Gałka, and Z. Hadzibabic, Universal Coarsening in a Homogeneous Two-Dimensional Bose Gas, arXiv:2312.09248 (2023).
- [46] M. P. Heller, A. Mazeliauskas, and T. Preis, Prescaling Relaxation to Nonthermal Attractors, *Phys. Rev. Lett.* **132**, 071602 (2024).
- [47] Y. Pomeau, Long term-long range dynamics of a classical field, *Phys. Scr.* **T67**, 141 (1996).
- [48] C. Eigen, A. L. Gaunt, A. Suleymanzade, N. Navon, Z. Hadzibabic, and R. P. Smith, Observation of Weak Collapse in a Bose-Einstein Condensate, *Phys. Rev. X* **6**, 041058 (2016).
- [49] M. R. Andrews, C. G. Townsend, H.-J. Miesner, D. S. Durfee, D. M. Kurn, and W. Ketterle, Observation of Interference Between Two Bose Condensates, *Science* **275**, 637 (1997).
- [50] A. Ramanathan, S. R. Muniz, K. C. Wright, R. P. Anderson, W. D. Phillips, K. Helmerson, and G. K. Campbell, Partial-transfer absorption imaging: A versatile technique for optimal imaging of ultracold gases, *Rev. Sci. Instrum.* **83**, 083119 (2012).
- [51] J. Etrych, G. Martirosyan, A. Cao, J. A. P. Glidden, L. H. Dogra, J. M. Hutson, Z. Hadzibabic, and C. Eigen, Pinpointing Feshbach resonances and testing Efimov universalities in ^{39}K , *Phys. Rev. Res.* **5**, 013174 (2023).
- [52] G. Martirosyan, C. J. Ho, J. Etrych, Y. Zhang, A. Cao, Z. Hadzibabic, and C. Eigen, Observation of Subdiffusive Dynamic Scaling in a Driven and Disordered Bose Gas, *Phys. Rev. Lett.* **132**, 113401 (2024).
- [53] Y. Kagan, B. V. Svistunov, and G. V. Shlyapnikov, Effect of Bose condensation on inelastic processes in gases, *JETP Lett.* **42**, 209 (1985).

METHODS

Optical box trap

Our cylindrical optical box is made of 532nm light. Our standard box of volume $V = 61 \times 10^3 \mu\text{m}^3$, used for most measurements, has radius $R = 22 \mu\text{m}$ and length $L = 40 \mu\text{m}$. For the additional measurement with the smaller $V = 17 \times 10^3 \mu\text{m}^3$, we use a box with $R = 14.5 \mu\text{m}$ and $L = 26 \mu\text{m}$. Note that in both cases $V^{1/3} \approx 2R \approx L$.

Measuring the momentum distribution $n_k(k)$

Our experiments are performed with the lowest hyperfine ground state of ^{39}K . We measure $n_k(k)$ after a time of flight (ToF) expansion, first optically pumping the atoms to the highest hyperfine ground state and then imaging them. To deduce n_k values that vary over 6 orders of magnitude, we combine measurements with ToF duration in the range (16–120) ms; the longest ToF minimises finite-size effects at low k , while shorter ones give better signal-to-noise at large k . Even for our longest ToF, the optical density (OD) at $k \approx 0$ is high for clouds with a high condensed fraction, so to deduce high column densities while keeping $\text{OD} \lesssim 2$, we pump a variable fraction of atoms (down to $\approx 3\%$) into the imaging state [50].

Initial-state preparation protocols

To prepare our initial states $P_{1,2,3}$, we start with a weakly interacting quasi-pure condensate with $N = 3 \times 10^5$ atoms [48], turn off the interactions ($a \rightarrow 0$) using the Feshbach resonance at 402.7 G [51], and perturb the cloud using a combination of time-dependent forcing and interaction pulsing, as outlined in Extended Data Fig. 1. The forcing parameters are chosen such that $P_{1,2,3}$ all have the same energy per particle, $\varepsilon = k_B \times 20 \text{nK}$.

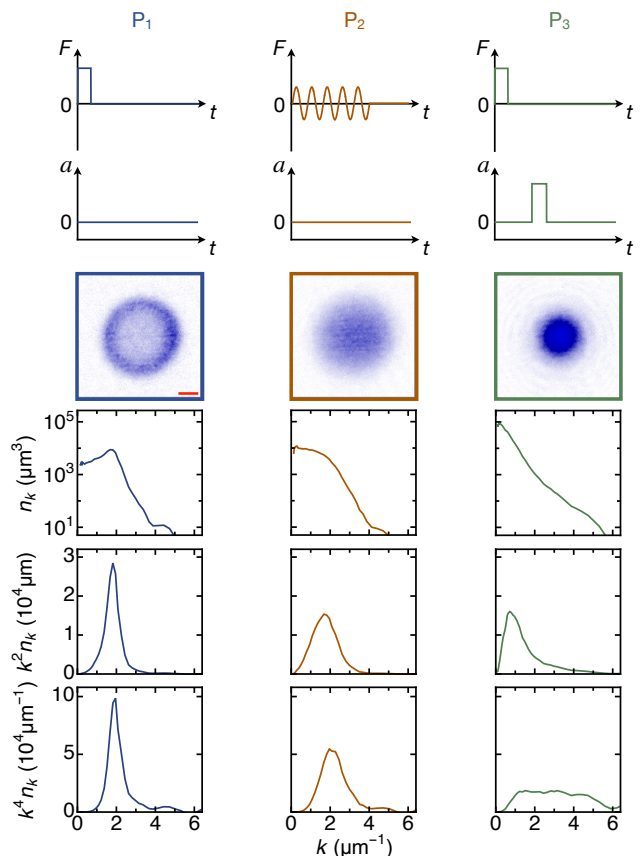
In a clean cylindrically symmetric potential, our forcing would result in anisotropic momentum distributions. However, weak disorder that is naturally present in our trap [52] couples excitations along different directions, so simply waiting for 500ms at $a = 0$ always results in states with isotropic, but far from equilibrium n_k .

The scaling exponent β

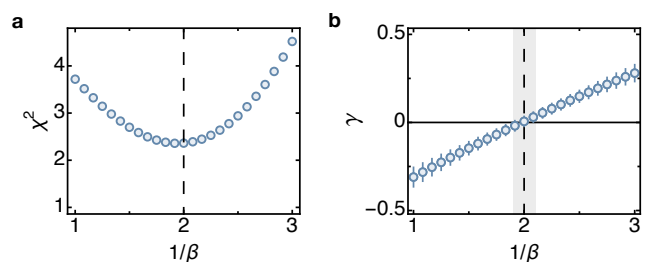
In the main paper we show that our data is consistent with $\beta = 1/2$. Here we provide additional analysis to confirm this.

First, at long times $\ell^{1/\beta}(t)$ is $\propto t - t^*$ only for the correct β . We perform such linear fits for all our 14 data series (see Fig. 3) assuming different values of β , and in Extended Data Fig. 2a show the combined χ^2 values for all 14 fits, which show a clear minimum near $1/\beta = 2$.

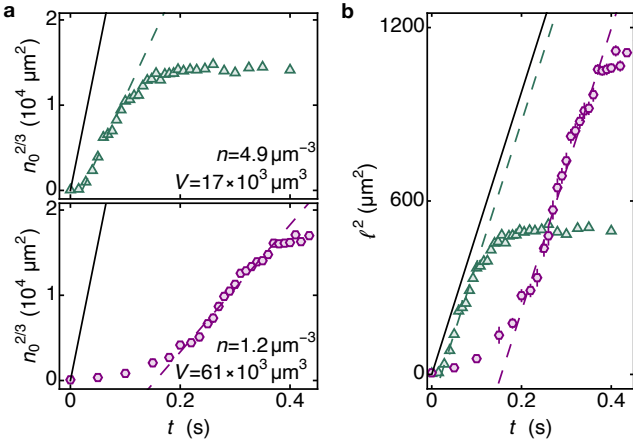
Second, ignoring the linear-fit quality for different β values, for self-consistency $d\ell^{1/\beta}/dt$ should be $\propto (na)^{1-1/(2\beta)}$ [Eq. (2)], so $C = (na)^{1/(2\beta)-1} d\ell^{1/\beta}/dt$ should be independent of na . Fitting $C \propto (na)^\gamma$ for all 14 data sets, we obtain $\gamma(\beta)$ shown in Extended Data Fig. 2b. We see that the results are self-consistent ($\gamma = 0$ within errors) only for $\beta = 0.50(3)$.



Extended Data Fig. 1. **Initial-state preparation.** We prepare our initial states using a combination of time-dependent force F and interaction pulsing, as shown in the top two rows. The forcing pulses for P_1 and P_3 are 8ms long and have strength $F_0 = k_B \times 1.5 \text{nK}/\mu\text{m}$. The sinusoidal force for P_2 has amplitude $F_0 = k_B \times 0.3 \text{nK}/\mu\text{m}$ and angular frequency $\omega = 2\pi \times 10 \text{Hz}$, and is applied for 1s. For P_3 the interactions are pulsed to $a = 400 a_0$ for 30ms. After the end of the preparation sequence we wait for 500ms at $a = 0$ for n_k to become isotropic. The images (same as in Fig. 1b) show the $k_x - k_y$ distributions for $k_z \approx 0$ just before we turn on interactions to initiate the relaxation; the red scale bar in the left image shows $1 \mu\text{m}^{-1}$. The bottom three rows show different moments of the corresponding momentum distributions. The integrals of $k^2 n_k$ and $k^4 n_k$ are, respectively, proportional to the total atom number and energy, which are the same for all three states.



Extended Data Fig. 2. **Determining β .** **a**, The χ^2 values (combined for all 14 data series summarised in Fig. 3) for the linear long-time fits of $\ell^{1/\beta}(t)$, showing a clear minimum at $1/\beta \approx 2$. **b**, The exponent γ quantifying the self-consistency of the dependence of $d\ell^2/dt$ on na for various $1/\beta$ (see text). Self-consistency requires $\gamma = 0$, which we observe for $\beta = 0.50(3)$ (grey shading).



Extended Data Fig. 3. **Changing V or n .** **a**, The rate of growth of $n_0^{2/3}$ in the scaling regime depends on both the system size (top) and the gas density (bottom). For reference, the solid black line shows the scaling-regime slope for our standard $n = 4.9 \mu\text{m}^{-3}$ and $V = 61 \times 10^3 \mu\text{m}^3$. **b**, However, the rate of growth of $\ell^2 = (Vn_0/n_0^{\text{eq}})^{2/3}$ in the scaling regime is universal. The only effect of the system size is that for lower V the finite-size saturation of ℓ^2 occurs at a lower value.

Data for different V and n

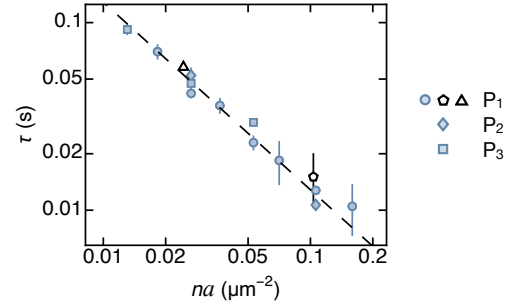
For two of the measurements summarised in Fig. 3 we reduced either V or n (while keeping ε the same) to show that this does not affect the value of the speed limit D . In Extended Data Fig. 3 we show further details of these measurements, which also highlight the fact that ℓ is the fundamental quantity that characterises coarsening. In the first case, reducing V while keeping n the same, keeps T_c and the equilibrium condensed fraction η^{eq} the same, but reduces the equilibrium $N_0 = \eta^{\text{eq}} n V$ and $n_0^{\text{eq}} = (2\pi)^{-3} \eta^{\text{eq}} n V^2$. In the second case, reducing n reduces T_c and hence η^{eq} , again reducing n_0^{eq} . Hence, in both cases the scaling dynamics of $n_0^{2/3}$ are different than for our standard V and n (see Extended Data Fig. 3a). However, the scaling dynamics of ℓ^2 are universal (see Extended Data Fig. 3b).

The timescale τ for the approach to the scaling regime

In the main paper (inset of Fig. 4b) we show that for all our P₁ data series the approach to the universal scaling regime is captured well by an exponential with a time constant $\tau \approx 50 t_\xi$, where $t_\xi \equiv m \xi^2 / \hbar = m / (8\pi \hbar n a)$. Here, in Extended Data Fig. 4, we show the results of independent exponential fits of all 14 series taken with different initial states (as summarised in Fig. 3). Fitting $\tau \propto (na)^\delta$ with a free exponent δ (dashed line) gives $\delta = -0.94(6)$, consistent with $\tau \propto t_\xi \propto 1/(na)$. Fitting the data with fixed $\delta = -1$ (not shown) gives $\tau = 52(2) t_\xi$.

Three-body losses

To study coarsening in an isolated system, we restricted our measurements to interaction strengths where the loss due to three-body recombination is not significant. For a



Extended Data Fig. 4. **The timescale for the approach to the scaling regime.** The timescale τ of the exponential fits to the data before the scaling regime, for all 14 data sets summarised in Fig. 3. The dashed line is a power law fit to the data, giving $\tau \propto (na)^{-0.94(6)}$, consistent with $\tau \propto t_\xi \propto 1/(na)$.

homogeneous weakly interacting Bose gas, this loss rate is

$$\frac{dn}{dt} = -\frac{3Z_3 \hbar n^3 a^4}{m}, \quad (\text{S1})$$

where the dimensionless Z_3 weakly depends on a and is ≈ 5 for our system, taking into account the suppression of density fluctuations for $\ell \gtrsim \xi$ [51, 53]. In order for these losses not to interfere with the coarsening, one requires

$$\frac{1}{\ell^2} \frac{d\ell^2}{dt} \gg \left| \frac{1}{n} \frac{dn}{dt} \right|. \quad (\text{S2})$$

For $d\ell^2/dt = 3\hbar/m$, this simplifies to $Z_3 n^2 a^4 \ll 1/\ell^2$, or

$$na^3 \ll \frac{8\pi}{Z_3} \left(\frac{\xi}{\ell} \right)^2. \quad (\text{S3})$$

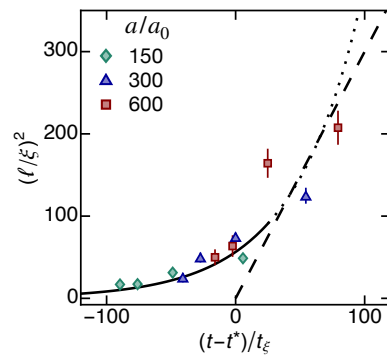
For this inequality to hold deep in the coarsening regime, $(\ell/\xi)^2 \sim 10^3$ (see Fig. 4c), one requires $na^3 \ll 5 \times 10^{-3}$.

Comparison to previous measurements

The early experiments on condensation dynamics were performed with inhomogeneous gases in harmonic traps [13, 15–18], which makes comparison with uniform-system theory difficult. The closest to probing the uniform-system physics was Ref. [16], where the emergence of coherence in a ^{87}Rb gas was probed interferometrically and the authors focused on the quasi-homogeneous region near the trap centre. Still, for a quantitative comparison, a problem is that in a harmonic trap the central density grows, and hence ξ decreases, during condensation. We therefore make only a rough comparison to our results. In Ref. [16], coherence spread over $8.5 \mu\text{m}$ in about 350 ms. However, consistent with our observation that initially the growth of ℓ/ξ accelerates (which should be even more pronounced for a continuously decreasing ξ), most of the dynamics happened in the final 100 ms, which gives an estimate $d\ell^2/dt \approx 0.7 \mu\text{m}^2/\text{ms}$, about three times lower than the ^{87}Rb speed limit, $D = 3\hbar/m_{\text{Rb}} \approx 2 \mu\text{m}^2/\text{ms}$.

In Ref. [43] (by our group), relaxation was studied in a box trap and for tunable interactions. The box size and the range of a values were similar to ours, but the initial

far-from-equilibrium state was prepared by rapid evaporation, removing 77% of the atoms, so the gas density and the observable values of ℓ/ξ were lower. The data were within errors consistent with dynamic scaling, but the deduced $\beta \approx 0.35$ was slightly lower than the expected $1/2$, and the characteristic relaxation time was $\propto 1/a$. However, as with all the NTFP experiments prior to Ref. [45], the approximation $|t^*| \ll t$ was implicitly assumed. Re-analysing these measurements, in Extended Data Fig. 5 we show that the data can be aligned with our results in Fig. 4b simply by including appropriate time shifts t^* , and the observed a -dependence of the relaxation dynamics is explained by the system not having reached the universal speed limit. All the data are consistent with the exponential growth, $(\ell/\xi)^2 \propto \exp[t/\tau]$, with $\tau = 50t_\xi \propto 1/(na)$, and the range of ℓ^2 values was the same for the three data sets with different a values. Hence, assuming a time-independent coarsening speed for each a individually gives $d\ell^2/dt \propto 1/\tau \propto a$.



Extended Data Fig. 5. **Comparison to the data from Ref. [43].** We present the data corresponding to Fig. 3 in Ref. [43] in the style of our Fig. 4b, and show that they are consistent with our results if we include appropriate time shifts t^* (which were not considered in Ref. [43]). The solid and dashed lines are the same as in Fig. 4, and the dotted one is the extension of the former. For the largest a , the data reaches $(\ell/\xi)^2 \approx 200$, but is still equally consistent with the speed limit $3\hbar/m$ (dashed line) and with the extrapolation of the initial exponential growth (dotted line).